

# Blue Stragglers form (most likely) via mass transfer

NATALIE M. GOSNELL<sup>1,2</sup>, ROBERT D. MATHEU<sup>3</sup>, AARON M. GELLER<sup>3,4</sup>, ALISON SILLS<sup>5</sup>,

NATHAN LEIGH<sup>6,7</sup>, AND CHRISTIAN KNIGGE<sup>8</sup>

<sup>1</sup> Department of Astronomy, The University of Texas at Austin, 2515 Speedway, Stop C1400, Austin, TX 78712-1205, USA; gosnell@astro.as.utexas.edu

<sup>2</sup> Department of Astronomy, University of Wisconsin—Madison, 475 N. Charter Street, Madison, WI 53703, USA

<sup>3</sup> Center for Interdisciplinary Exploration and Research in Astrophysics (CIERA) and Department of Physics and Astronomy, Northwestern University, 2145 Sheridan Road, Evanston, IL 60208, USA

<sup>4</sup> Department of Astronomy and Astrophysics, University of Chicago, 5640 S. Ellis Avenue, Chicago, IL 60637, USA

<sup>5</sup> Department of Physics and Astronomy, McMaster University, 1280 Main Street W, Hamilton, ON L8S 4M1, Canada

<sup>6</sup> Department of Physics, University of Alberta, CCIS 4-183, Edmonton, AB T6G 2E1, Canada

<sup>7</sup> Department of Astrophysics, American Museum of Natural History, Central Park West and 79th Street, New York, NY 10024, USA

<sup>8</sup> School of Physics and Astronomy, University of Southampton, Highfield, Southampton, SO17 1BJ, UK

Received 2015 June 11; accepted 2015 October 6; published 2015 December 1

"BSSS"

## Abstract

We present results of a *Hubble Space Telescope* (*HST*) far-ultraviolet (FUV) survey searching for white dwarf (WD) companions to blue straggler stars (BSS) in open cluster NGC 188. The majority of NGC 188 BSSs (15 of 21) are single-lined binaries with properties suggestive of mass-transfer formation via Roche lobe overflow, specifically through an eccentric giant branch orbit that has evolved to a near-circular configuration, yielding a BSS binary with a WD companion. In NGC 188, the BSS+WD binary population formed by this mechanism in the past 400 Myr will have a WD companion that is hot and luminous enough to be directly detected as a FUV photometric excess with *HST*. Comparing expected BSS FUV emission to observed photometry, we find 14 BSSs with WD companions above 12,000 K, ranging from 11,000 to 12,000 K. The BSS+WD binaries are all formed through recent mass transfer. The location of the young BSSs in an optical color-magnitude diagram (CMD) indicates that distance from the zero-age main sequence does not necessarily correlate with BSS age. There are no CMD features that distinguish mass-transfer-formed BSSs and those likely formed through other mechanisms, such as collisions. The seven detected WD companions place a lower limit on the mass-transfer formation frequency of 33%. We consider other possible formation mechanisms by comparing the ages of the BSSs with their typical pre-main sequence lifetimes, finding a value likely formed from mass transfer, resulting in an inferred mass-transfer formation frequency of approximately 1%.

**Key words:** binaries: spectroscopic – blue stragglers – open clusters and associations: individual (NGC 188) – ultraviolet: stars – white dwarfs

## what do we know about BSS?

Open clusters are ideal environments for studying stellar populations. The ability to isolate a single stellar population from the field using radial-velocity (RV) and proper-motion measurements not only informs our understanding of normal stellar populations, but also highlights those stars whose evolutionary paths deviate from single-star expectations. One such group of stars is blue straggler stars (BSSs). Traditionally defined as cluster members that are brighter and bluer than the corresponding main sequence turnoff (Sandage 1953), the definition extends to stars that appear to be evolving given the cluster age, such as stars below the turnoff but bluerward of the main sequence (Mathieu & Geller 2000). BSSs are not anomalous objects; they are found in open clusters (e.g., Johnson & Sandage 1955; Boissé & Sandage 1958; Leonard 1996; Sandquist 2005; Talamantes et al. 2010), globular clusters (Sandage 1953; Ferraro et al. 1999; Piotto et al. 2004; Leigh et al. 2007; Knigge et al. 2009; Santana et al. 2013), the Galactic field (Preston & Sneden 2000; Carney et al. 2001), and dwarf galaxies (Mapelli et al. 2007; Momany et al. 2007). The BSS population of open cluster NGC 188 is in addition to a few subgiants and yellow dwarfs, comprising roughly 25% of the evolution-

population (Mathieu & Geller 2014, and references therein). Thus, understanding the creation and subsequent evolution of BSSs is of particular standard stellar astrophysics, fundamental to constraining the nature of stellar evolution at large.

BSSs were first discovered about 60 years ago (Sandage 1953; Johnson & Sandage 1955), and understanding their formation continues to be an active field of research. A common theme is that BSS components may gain additional mass through a stellar or binary interaction, either by robbing mass from another star about the main sequence turnoff, but theories differ on how this is acquired. There are currently three primary theories for binary BSS formation: stellar collisions during dynamical interactions of binaries with single stars or other binaries (e.g., Leonard 1989; Ferraro et al. 1995; Merritt & Heggie 1996; Dehnen & Staeblein 1997), formation of an inner binary in a triple system via the Yozai mechanism (Deets & Fabrycky 2009; Naoz & Fabrycky 2014; Antonini et al. 2015), and Roche lobe overflow mass transfer while the original primary star is still on the main sequence.

(A) *asymptotic giant branch* (AGB), Case C; e.g., McCrea 1964; Ferraro et al. 2001, 2006; Chen & Han 2008; Leigh et al. 2011, 2013; Gosnell et al. 2014). Although not a likely pathway for young BSSs, mass transfer while both stars are on the main sequence can occur in Case C, creating the excess (Webbink 1976; Lombardi et al. 2002).

Found in star field and dwarf galaxies.

# It is important for a full stellar evol. picture!!

THE ASTROPHYSICAL JOURNAL, 814:163 (12pp), 2015 December 1

GOSSELL ET AL.

(BSSs) Finally, all these formation scenarios create BSSs similar to those observed in star clusters, but the details of the BSS population will vary. Collision can create single BSSs or binary BSSs via a close dynamical encounter (Leigh & Geller 2011; Leigh & Geller 2012). In this work, a collision product is a star resulting from a collision, coalescence, or merger of two stars during a dynamical encounter, formed through Case A mass transfer typically with a tertiary companion (Webbink 1979; Lombardi et al. 2006), although Tian et al. (2006) model the formation of BSSs from Case A mass transfer that result in binaries with periods less than 10 days. The Kozai mechanism will create a binary BSS whose secondary is the original tertiary member of the system (Perets & Farysky 2009). A BSS formed from a collision or overflow will also be in a binary, but its secondary will be the core of the progenitor primary star, observed as a carbon/oxygen (CO) or helium white dwarf (WD; Geller & Mathieu 2011; Geller et al. 2013; Gosnell et al. 2014).

The number of BSSs observed in a star cluster is determined by a combination of the formation rate for a given mechanism and the corresponding BSS completeness. N-body models are capable of predicting the numbers of BSSs in cluster environments, and through each formation method (Hurley et al. 2005; Geller et al. 2011). However, empirical determination of BSS formation for a given population is necessary in order to make appropriate comparisons to N-body model results.

Observational identification of the particular formation mechanisms for an entire population of BSSs has proved elusive, although several pathways for several individual BSSs have been determined in globular clusters. Knigge et al. (2008) find a globular cluster BSS+WD binary that perhaps formed through mass transfer (although it may also be the result of a dynamical exchange) and Roig et al. (2013) find a globular cluster BSS currently undergoing mass transfer. In 47 Tuc, Ferraro et al. (2013) discover a BSS with a detached CO that is suggestive of a mass transfer history, and Knigge et al. (2006) find a BSS originally formed from at least three stars, but (by design) none of these studies provide enough context to learn about the formation mechanisms of the entire BSS population. In globular cluster M30, Ferraro et al. (2009) find a trend in optical color and magnitude that suggests two BSS sub-populations split between mass transfer and possibly formed products, but further observational constraints such as detecting BSS binarity, is very difficult due to the crowded nature of globular clusters (e.g., Brodtkorb et al. 2011; Matheny et al. 2012). In the case of globular cluster NGC 188, Buciksa (2001) provides evidence that mass transfer must be responsible for at least a portion of the BSS population.

In an attempt to disentangle the problem of multiple formation pathways, we focus on the population of BSSs in open cluster NGC 188, which presents an excellent environment for studying these objects. The cluster is one of the oldest known open clusters in the Galaxy, with an age of 7 Gyr (Sarajedini et al. 1999). The BSSs, therefore, are not very "old" allowing for accurate RV measurements and binary membership (Geller et al. 2009). The BSSs are also relatively low-mass (77–78 solar mass), so space is not prohibitively small for binary formation. This study

(Mathieu et al. 2009) has observed NGC 188 for almost 20 years, obtaining a proper motion (Sarajedini et al. 1999), radial velocities (Platais et al. 2009), and RVs (Geller et al. 2009). Our efforts with sophisticated binary models covering the entire cluster lifetime (Geller et al. 2011), this enormous foundation of data makes the NGC 188 BSS population one of the most well-studied in the Galaxy.

NGC 188 has 42 BSSs, 20 of which are high-probability three-dimensional cluster members (Geller et al. 2003; Geller et al. 2008). The single exception, WOCS 42, is a binary star photometrically classified as a BSS but lacks orbital parameters, orbit duration, and mass, resulting in unknown, 100-determined cluster membership. Geller et al. (2003) determine a proper motion membership probability for WOCS 42 ( $\sim 3\%$ ). The majority (80%) of the BSSs in NGC 188 are spectroscopic (Mathieu & Geller 2009). Four BSSs do not have detected radial variability, meaning they are not in binaries with orbital periods less than  $10^4$  days (Geller et al. 2009). These stars have periods as long as  $10^6$  days ( $P_{\text{orb}} \sim 10^6$  days) or are detached (Geller & Mathieu 2012). Binaries with periods beyond  $10^4$  days are thought to be destroyed through dynamical interactions in the cluster environment. The BSS population includes two double-lined spectroscopic binaries with short orbital periods (Mathieu & Geller 2009), a high-velocity runaway with a period of  $q = 0.0001$  (Geller et al. 2009). The remaining 15 BSS binaries are single-lined, which we refer to as SB systems. Table 1 summarizes the NGC 188 BSS population, including the cluster identifier (WOCS ID), J2000 location, optical photometry and color, membership class, and effective temperature. In addition we include the orbital period and eccentricity for binary BSSs with orbital solutions.

The binary parameters of the SB systems are striking. All but one of the SB1 BSSs have periods within a factor of 2–3 of 1000 days, compared to the main sequence period distribution that extends from a few days up to several thousand days (Mathieu & Geller 2009). The statistical secondary mass distribution has a sharp peak at  $0.5 M_{\odot}$ , that is distinct from the mass distribution of the main sequence secondary stars at the 99% confidence level. This suggests the companions are CO WDs, whose masses are typically around  $0.5 M_{\odot}$  (Geller & Mathieu 2011). These binary parameters are consistent with the mass transfer occurring through Case C mass transfer (Chen & van der Klis 2004).

We seek to observationally detect these potential companions with a far-ultraviolet (FUV) photometric campaign using the *Hubble Space Telescope* (HST). The first results of this study are presented in this paper. We will also identify the BSSs with potential companions and present specific formation scenarios for each system. The shorter periods ( $\sim 1370$  to  $120$  days) are possible due to Case C mass transfer and the mass loss of the WD, also covered in Gosnell et al. (2014).

In the next section, we review the results of the HST data for remnant WDs and their companions and discuss the implications for the frequency of different BSS formation mechanisms. We present our detection limits and photometric analysis of the BSS population. In Section 4, we detect WD companions in Section 3, discuss the frequency of mass transfer formation and implications for modeling efforts in Section 4, and summarize our study in Section 5.

*already observed*

groups

21!

**Table 1**  
NGC 188 Blue Straggler Star Population

ID	Position (J2000)	$V^a$	$B - V^a$	Class <sup>b</sup>	$T_{\text{eff}}^c$	$P_{\text{orb}}$ (days) <sup>b</sup>	Eccentricity <sup>b</sup>
<i>Non-velocity Variable:</i>							
1366	00:51:15.06, +85:44:02.02	15.851	0.620	SM	6120 ± 120	...	...
4290	00:42:06.53, +85:16:47.25	14.174	0.584	SM	6280 ± 90	...	...
4306	00:42:20.59, +85:15:39.47	13.347	0.534	SM	6450 ± 100	...	...
5020	00:47:51.46, +85:15:09.09	14.000	0.502	SM	6750 ± 130	...	...
<i>Single-lined Binaries:</i>							
451	00:34:47.95, +85:32:27.33	13.880	0.604	BM	6400 ± 110	722 ± 4	...
1888	00:54:31.35, +85:32:09.12	14.841	0.552	BM	6570 ± 120	2240 ± 30	0.21 ± 0.04
2679	00:26:44.64, +85:18:35.94	15.011	0.515	BM	6630 ± 120	1033 ± 8	0.07 ± 0.05
4230	00:43:23.81, +85:20:32.64	15.269	0.534	BU	6350 ± 110	...	...
4348	00:43:41.47, +85:13:17.28	14.780	0.540	BM	6750 ± 120	1168 ± 8	0.09 ± 0.05
4540	00:45:18.27, +85:19:19.85	13.851	0.517	BM	6520 ± 100	3030 ± 70	0.36 ± 0.07
4581	00:45:56.63, +85:17:29.66	14.147	0.521	BM	6750 ± 120	546.7 ± 1.6	0.269 ± 0.015
4589	00:46:22.99, +85:17:13.46	14.995	0.595	BM	6240 ± 100	615.2 ± 1.7	0.21 ± 0.04
4970	00:47:13.32, +85:16:39.87	14.524	0.622	BM	6170 ± 90	1002.76 ± 2.4	0.095 ± 0.013
5325	00:35:06.67, +85:16:51.20	15.250	0.540	BM	6400 ± 110	1772 ± 12	0.77 ± 0.03
5326	00:35:04.05, +85:14:38.08	15.372	0.570	BM	6400 ± 110	690 ± 3	0.07 ± 0.03
5434	00:48:54.45, +85:12:36.71	14.687	0.526	BM	6550 ± 110	120.21 ± 0.04	0.24 ± 0.03
5671	00:52:25.78, +85:15:27.80	15.609	0.659	BM	6130 ± 90	1277 ± 9	0.551 ± 0.018
8104	00:40:15.45, +85:03:23.00	15.260	0.540	BM	6170 ± 110	1423 ± 7	0.286 ± 0.018
<i>Double-lined Binaries:</i>							
5078	00:47:11.69, +85:13:31.00	14.061	0.501	BM	...	4.78303 ± 0.00012	0.121 ± 0.0006
7782	00:35:46.23, +85:14:14.00	14.780	0.540	BM	...	5.32770 ± 0.00005	0.013 ± 0.006

Notes.

<sup>a</sup> Sarajedini et al. (1999).<sup>b</sup> Gossnell et al. (2014). Class codes are SM: Single Member, BM: Binary Member, and BU: Binary other motion member, but no orbit or RM member.<sup>c</sup> Estimated from the color-magnitude diagram fit using the same equation from Geller et al. (2014) and Section 3.

companion masses  $\sim 0.5 M_{\odot}$   
 CO WDs?  


→ BSSs formation through case C

## OBSERVATIONS

Our observations were carried out using the HST Advanced Camera for Surveys (ACS) in the Solar Blind Channel (SBC). The observations occurred in 19.5 s 2- or 3- orbit intervals between 2012 October 11 and November 12, 2012 (M1, P1; Matthei). We did not include the two SB1 BSSs in this study as their high mass ratios make determining secondary stars indicate the companions are not WDs (Geller et al. 2014; Matthei & Geller 2009). An additional star, WOCS 1947, was included in the HST study but Matthei & Geller (2014) later found it to be a red giant star. A visual photometric color in the literature caused the erroneous categorization of this source. We refer to WOCS 1947 in Section 2.1.1.

Each BSS was observed in F410LP for 2040 s, F150LP for 2380 s, and F165LP for 1564 s. The total exposure times are the sum of four short exposures using the standard ACS/SBC 4-point box filter pattern. We also utilize derived narrow bandpasses to better isolate the bluest FUV flux. We exploit the nested nature of the long-pass filters by differencing F140LP and F150LP to create F140N, and differencing F150LP and F165LP to create F150N (Dieball et al. 2005; Gossnell et al. 2014).

The SBC field of view is very small at  $25'' \times 25''$ . In all but one case the BSS target is the only star visible in the SBC image; therefore the images do not suffer from source confusion or blending.

Done with  
this bad boy

Top 19 BSS

2.1.1. ACS Red Leak

The ACS/SBC has a known red leak beyond 2000 Å (Boff et al. 2006; Renteria 2007). We use the red leak model of Feldman et al. (2010) as it is the most accurate (Feldman et al. 2010). Although the SBC detector temperature rises with continued use, we find no systematic correlation in flux ratio for temperature and red leak flux for each exposure for each filter.

In the absence of identifying the red leak trend we use the simultaneous observation of the red giant WOCS 1947 (Geller et al. 2014) to estimate the red leak. Using the color  $B - V = 1.29$  (Henden & Munari 2014), we assume all of the SBC flux for WOCS 1947 is due to the red leak. We estimate the red leak contribution of each BSS by scaling the detected red leak flux of WOCS 1947 in each long-pass filter by  $V$ -band luminosity. We then subtract off the “extra” red leak flux. This results in count rates that, to the best of current capabilities, are

<sup>a</sup> <http://www.stsci.edu/hst/observatory/focus/TinyTim>

Table 2  
*HST* FUV Photometry of NGC 188 BSS Population

WOCS ID	NUV <sup>a</sup>	F165LP	F150LP	F140LP	F150N <sup>b</sup>	F140N <sup>b</sup>
451	18.38 ± 0.04	18.94 ± 0.04	20.06 ± 0.03	20.54 ± 0.03	22.2 <sup>+0.5</sup> <sub>-0.5</sub>	23.2 <sup>+0.7</sup> <sub>-0.9</sub>
1366	20.6 ± 0.2	20.63 ± 0.07	21.83 ± 0.05	22.62 ± 0.06	25.5 <sup>+1.7</sup> <sub>-1.7</sub>	...
1888	19.39 ± 0.07	19.78 ± 0.05	20.72 ± 0.04	21.37 ± 0.04	21.9 <sup>+0.3</sup> <sub>-0.4</sub>	...
2679	19.07 ± 0.06	19.22 ± 0.04	20.31 ± 0.05	20.67 ± 0.03	21.5 <sup>+0.3</sup> <sub>-0.3</sub>	22.7 <sup>+0.4</sup> <sub>-0.8</sub>
4230	19.49 ± 0.07	19.78 ± 0.05	20.31 ± 0.05	20.77 ± 0.03	21.5 <sup>+0.3</sup> <sub>-0.3</sub>	22.6 <sup>+0.6</sup> <sub>-0.6</sub>
4290	19.02 ± 0.06	19.22 ± 0.04	20.62 ± 0.05	20.90 ± 0.03	22.3 <sup>+0.4</sup> <sub>-0.7</sub>	...
4306	18.00 ± 0.04	18.23 ± 0.03	19.29 ± 0.07	20.22 ± 0.04	20.9 <sup>+0.3</sup> <sub>-0.3</sub>	...
4348	18.59 ± 0.05	18.61 ± 0.03	19.55 ± 0.02	20.00 ± 0.04	20.6 <sup>+0.2</sup> <sub>-0.3</sub>	21.4 <sup>+0.3</sup> <sub>-0.3</sub>
4540	18.17 ± 0.04	17.96 ± 0.02	18.58 ± 0.01	18.80 ± 0.01	19.07 <sup>+0.09</sup> <sub>-0.07</sub>	19.29 <sup>+0.05</sup> <sub>-0.03</sub>
4581	18.47 ± 0.04	18.61 ± 0.02	19.54 ± 0.02	20.41 ± 0.03	21.6 <sup>+0.3</sup> <sub>-0.3</sub>	...
4589	19.77 ± 0.09		21.34 ± 0.05	21.86 ± 0.05	24.1 <sup>+0.0</sup> <sub>-0.0</sub>	...
4970	19.63 ± 0.08	19.95 ± 0.06	20.96 ± 0.04	21.53 ± 0.05	22.4 <sup>+0.4</sup> <sub>-0.7</sub>	...
5020	18.09 ± 0.04	18.19 ± 0.03	19.21 ± 0.02	19.71 ± 0.02	20.7 <sup>+0.2</sup> <sub>-0.2</sub>	22.7 <sup>+0.6</sup> <sub>-1.6</sub>
5325	19.78 ± 0.09	19.96 ± 0.05	20.98 ± 0.04	21.63 ± 0.04	22.5 <sup>+0.5</sup> <sub>-0.5</sub>	...
5350	17.63 ± 0.03	17.50 ± 0.02	18.49 ± 0.01	18.97 ± 0.01	19.9 <sup>+0.1</sup> <sub>-0.1</sub>	21.4 <sup>+0.2</sup> <sub>-0.4</sub>
5379	19.87 ± 0.09	19.13 ± 0.04	19.23 ± 0.02	19.26 ± 0.02	19.27 <sup>+0.05</sup> <sub>-0.06</sub>	19.31 <sup>+0.04</sup> <sub>-0.04</sub>
5434	19.00 ± 0.06	19.36 ± 0.04	20.53 ± 0.03	21.13 ± 0.04	23.4 <sup>+0.9</sup> <sub>-0.9</sub>	...
5671	18.80 ± 0.05	19.09 ± 0.04	20.17 ± 0.02	20.73 ± 0.03	22.0 <sup>+0.4</sup> <sub>-0.6</sub>	...
8104	19.69 ± 0.02 <sup>c</sup>	21.27 ± 0.11	22.15 ± 0.07	23.01 ± 0.09	23.1 <sup>+0.1</sup> <sub>-0.6</sub>	...

Notes.

<sup>a</sup> GALEX NUV magnitude (AB system), except where noted (Martin et al. 2005).

<sup>b</sup> Magnitudes in italics are less than 3 $\sigma$  detections.

<sup>c</sup> WFC3 F218W instrumental magnitude (this study).

red leak-free. The mean red leak correction in F150LP is 0.15 mag.

The de-reddened leak,  $\phi_{\text{red}}$ , for WOCS 1947 is about 1.1 predicted by the model with very high throughput (Modeling WOCS 1947 with an ATLAS9 spectrum (Castelli & Kurucz 2004) with an effective temperature of 4575 K and surface gravity,  $\log(g) = 5$ , the SYNPHOT model correctly calculates a leak of 1.2  $\text{counts s}^{-1}$  in the long-pass filters. This is in comparison to the measured count rates of 0.212 ± 0.009, 0.279 ± 0.009, and 0.2 ± 0.0 counts  $\text{s}^{-1}$  for F140LP, F150LP, and F165LP, respectively. The resulting magnitude difference is 0.9 ± 0.1 MAG in F150LP ( $M_{\text{synphot}} = 22.1$ ,  $M_{\text{obs}} = 21.2$ ). These observations also suggest that the red leak is not constant across the long-pass filters. The measured difference of the observed red leak compared to SYNPHOT is slightly less than the difference seen by Feldman et al. (2010). Using the SBC PR130L prism, they find the observed red leak throughput to be 2.5 times that of the SYNPHOT throughput curve.

### 2.1.2. Magnitude Calculation

Encircled energy-corrected and red leak-subtracted count rates are used to calculate instrumental magnitudes in the STMAG system. We convert the count rates into fluxes ( $\text{erg cm}^{-2} \text{s}^{-1} \text{\AA}^{-1}$ ) using the PHOTFLAM conversion factors for F140LP, F150LP, and F165LP provided in the ACS Data Handbook (Gonzaga et al. 2014). We find the count rates in F140N and F150N by differencing the corrected count rates of the long-pass filters, where F140N = (F140LP – F150LP) and F150N = (F150LP – F165LP). We calculate the flux conversion factors for F140N and F150N using SYNPHOT and the F140N and F150N flux errors by combining the flux errors of the long-pass filters in quadrature, scaled by the different exposure times. We calculate instrumental magnitudes in all

bandpasses using  $\text{STMAG} = -2.5 \log_{10}(\text{flux}) - 21.1$ . The photometric errors are dominated by Poisson noise due to low counts. The ACS/PR130L gain factor, and the signal is high enough that the error distributions are approximately symmetric for all but the faintest measurements in F140N and F150N.

*There is a very small field of view, so most targets are the only source visible (no source blending)*  
*Analysis*  
*The FUV Color-Magnitude Diagram*

Accurate modeling of the BSS population is a key factor in determining the amount of expected FUV emission. We take special care to match modeled and observed near-UV (NUV) photometry (see Section 3.2). We use GALEX NUV photometry for this purpose (Martin et al. 2005). However, one BSS in NGC 188, WOCS 8104, is not detected in GALEX. We obtained NUV photometry for WOCS 8104 using the *HST* WFC3 in F218W. The observation occurred on 2012 June 19 as part of this program, with a total exposure time of 669 s. We use DAOPHOT for source detection and aperture photometry, and calculate the instrumental F218W magnitude for WOCS 8104 (given in Table 2).

Identifying WD companions relies on detecting a FUV excess above the emission expected for a BSS alone. We first compare the observed photometry with modeled BSS photometry for the entire BSS population. This approach best

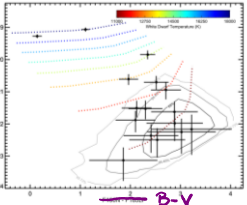


Figure 1. FUV CMD of the NGC 188 BSSs, shown in black with  $1\sigma$  error bars. The three BSSs with less than a  $3\sigma$  detection in F150N are not included in this figure. BSSs with solid distribution contours are shown in gray. The three main results are shown in black. The color bar indicates the temperature of the white dwarf. The dashed lines show synthetic spectra with temperatures varying from 11,000 to 16,000 K, as indicated by the color bar, with BSS temperatures varying from 5750 K (red end) to 6750 K (blue end) along each dashed line. Four BSSs are clearly seen to have a significant FUV excess and are separated from the BSS-only distribution by more than  $3\sigma$  (see also Gosnell et al. 2014).

demonstrates the general trend of FUV emission for the type of BSSs found in NGC 188 in comparison to the FUV emission from potential WD+WD pairs. It also highlights the three BSSs with high surface FUV luminosity, indicative of hot (temperatures greater than 12,000 K) WD companions.

In Figure 1 we plot the color-magnitude diagram (CMD) for the BSS population with two model spectra of the total BSS population and WD+WD pairing (described in detail in the next two sections). The observed BSS population is shown with black crosses and error bars. We use F150N–F160LP as our filter set. We exclude any BSS with less than a  $3\sigma$  detection in F140N in Figure 1 and in all subsequent analyses. This leaves us with 16 BSSs (5434, both stars and WDs) and one 'lonely' variable star (lack of a F140N detection). These three sources are considered to be outliers or contaminants in the NGC 188 sample.

The remaining BSS sample used for further analysis includes 16 BSSs (5434, both stars and WDs) and one variable star (lack of a F140N detection). These three sources are also having more than a  $3\sigma$  detection in F140N (WOCS 4540, 4348, and 5379) were presented in Gosnell et al. (2014), and are included in this sample of 16 BSSs.

## Modeling lonely BSSs

We calculate the FUV emission of the overall NGC 188 BSS population using a population synthesis approach including a large number of model spectra spanning the entire range of observed BSS temperatures and luminosities. The modeling is done through a three step process: (1) we establish the ranges of physical parameters that define the NGC 188 BSS population, (2) we create a large sample of model spectra constrained by those ranges, and (3) we calculate synthetic photometry for the sample of model spectra.

First, we define the range of parameters for the model spectra using the observed temperatures and luminosities of the NGC 188 BSSs.

The BSS temperatures are determined using metallicity-independent 4- or 5-band colors to constrain them from Ramirez & Meléndez (1998),  $E(B-V)$ ,  $V-H$ , and  $V-K$  (Sajadiani et al. 1999; Skrutskie et al. 2006).  $V-I$  is also used if FUV photometry is available. The resulting temperatures from the model spectra and the BSSs are given in Table 1. The errors given include the error in each color measurement and the systematic error in the temperature calculation as given in Ramirez & Meléndez (2005).

We use the luminosity range based on GALEX NUV magnitudes for which we have data (Munoz-Arias et al. 2007). The GALEX NUV photometry is the bluest luminosity information available it provides the most accurate normalization for creating the FUV spectra.

We will create 50,000 individual model spectra that, together, constitute the BSS-only model population. We create smooth probability density functions (PDFs) modeled after the observed shapes of BSS temperature and NUV luminosity cumulative distribution functions (CDFs). We Monte Carlo sample from these PDFs to create the model spectrum. There is only a weak correlation between temperature and luminosity in the NGC 188 BSS population ( $r = -0.2$ ) so they are sampled independently. For each sampling of the PDFs we calculate a model spectrum by interpolating between reddened UVBLUBE spectra with temperatures of 6000, 6500, 6750, and 7000 K to match the sampled temperature ( $E(B-V) = 0.09$ ,  $[Fe/H] = 0$ ,  $\log(g) = 3.5$ ; Sajadiani et al. 1999; Rodriguez-Merino et al. 2006). We then normalize the interpolated spectra in magnitude space and then use linear interpolation and random bin steps are carried out on all 50,000 PDF samples. As a result, we have a BSS-only model composed of a large set of model spectra spanning the range of physical parameters observed in the NGC 188 population.

Finally, after creating the BSS-only model we calculate the expected FUV CMD for the entire model distribution. We convolve each model spectrum with synphot F140LP, F150LP, and F160LP filters to derive the gain curves for the observed filters. The gain corrected throughput curves do not include a red noise component. We add Poisson noise to the convolutional dynamic range. The photon count ratio to the errors in FUV, F150LP, and F160LP are set in the same manner as the observations. We calculate magnitudes in F140LP, F150LP, F160LP, F140N, and F150N for each of the 50,000 spectra.

We compare the modeled BSS-only FUV photometry with the observed BSSs in Figure 2. Two-dimensional density histograms of model photometry are represented by gray contours enclosing 68%, 95.45%, and 99.7% of the distribution, as labeled. We restrict the density contours to those modeled sources that meet or exceed the same  $3\sigma$  F150N detection threshold we apply to the observations.<sup>10</sup>

<sup>10</sup> We note that a similar figure in Gosnell et al. (2014) does not have the same  $3\sigma$  detection cutoff, resulting in contours that extend fainter and redder than the contours shown here. In either case, the extent of the contours into the lower right corner of the CMD does not impact our search for WD companions.

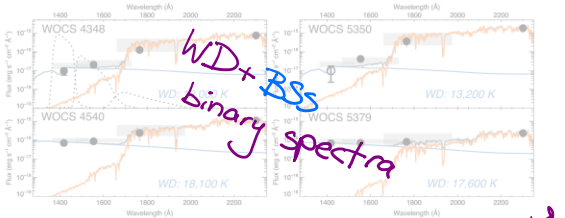


Figure 2. Best-fit BSS+WD spectra for the four BSS with hot WD companions, as labeled. The WD spectrum is shown in blue with the temperature as last. The mean BSS wavelength spectrum (given in Table 1) is shown in orange, and the combined BSS+WD spectrum is shown in dark gray. The synthetic photometry combined spectrum is shown with the light gray boxes. The vertical extent of the boxes shows the photometry range given the temperature uncertainty of the WD. The horizontal extent of the boxes represents the filter width, including the red tail of each bandpass. The upper left plot also includes the effective throughput and throughputs (black dashed lines) as a guide. The observed photometry in F140N, F150N, F165LP, and GALEX NUV is shown as filled black circles. The reference wavelength for each bandpass. Measurements in F140N that are below  $3\sigma$  are shown as an open circle. Observed fluxes are also plotted in black when the error exceeds the size of the symbol. The best-fit spectrum is required to match the GALEX NUV measurement.

BSS + WD Pairs

In order to demonstrate the presence of a WD companion changes in the BSS emission we create representative pairs of BSS+WD binaries. Keeping the BSS luminosity constant at GALEX NUV magnitude of 18.0 to mimic the brightest BSS in the NUV, we add together the spectra of BSSs between 3750 and 6750 K (Rodríguez-Merino et al. 2005) with WD temperatures ranging from 11,000 to 18,000 K. We use a D�para with  $\tau = 7.75$  (Wood 1995, P. Bergeron 2014 private communication). We calculate the synthetic photometry for each BSS+WD pair using the same method as for the BSS-only distribution.

The synthetic photometric results for the BSS+WD pairs are shown in Figure 1 as dotted lines. The rainbow colors indicate the WD temperature, which is colorbar. The length of each line segment corresponds to a particular WD temperature, with a BSS of 5750 K on the left (blue end) extending to a BSS of 6750 K on the right (red end). Since a higher WD temperature contributes more to the total BSS+WD it results in an overall redder color. The position of the rainbow triangles in the color-magnitude diagram shows that single BSS luminosity is sufficient to illustrate the general photometric trends for BSS+WD binaries.

Final analysis shows that there are four sources with obvious FUV excesses: WOCS 4348, WOCS 4540, WOCS 5350, and WOCS 5379. These sources are well separated from the BSS-only distribution and their photometry is consistent with the FUV excesses expected for BSS+WD binaries.

We fit BSS+WD spectra to estimate the FUV excess individually to estimate the minimum WD temperature. In Figure 2 we show the F140N, F150N, F165LP, and GALEX NUV photometric data for these sources. We fit a WD spectrum found through weighted least squares minimization. A similar figure for WOCS 4348, 4540, and 5379 is shown in Gosnell et al. (2014), although here we employ

an improved method of finding the best-fit WD temperature. The grid of WD models (Gosnell et al. 2015, see section 4) has a temperature resolution of 1000 K. In Gosnell et al. (2014) we restricted our search to grid temperature values within the two standard deviations between the WD models. Given the uncertainty in the true WD temperature, the results here and in Gosnell et al. (2014) are consistent. In each case the mean temperature BSS spectrum is shown in orange, the WD spectrum in blue, and the combined spectrum in gray. The synthetic photometry of the combined spectrum is shown with light gray boxes. The vertical extent of the boxes shows the photometric range given the temperature uncertainty of the WD. The horizontal extent of the boxes represents the filter width while the vertical extent shows the range in photometry including the FUV WD temperature uncertainty according to the GALEX NUV photometry. The narrowband effective throughputs are shown in the upper left plot as a guide. The observed photometry is shown in black circles. The reference wavelength for each bandpass and effective throughput factors are shown when they exceed the symbol size. Measurements in F140N that are less than  $3\sigma$  are shown with an open circle. The best-fit spectra are also checked for consistency with  $U$ -band photometry when available (Soderblom et al. 2014). We use the estimated temperature and uncertainty from Figure 2 to find the age of WDs and the mass loss rate (Heger & Bergeron 2006; Sana et al. 2012). In Table 2 we list the best-fit WD temperature estimates and the age range for each of the four BSSs with a hot WD companion, along with the observed binary period and eccentricity (Geller et al. 2009). Of these BSSs, the maximum age is  $230 \pm 30$  Myr for WOCS 4348, so all four BSSs formed very recently in comparison to the 7 Gyr age of NGC 188.

### 3.4. The FUV-faint BSS Sample

There are 12 remaining BSSs (nine binaries, three non-variable) within the sample of F150N sources that

# "Hot" WD parameters

Hot WD Companion Temperature and Age Estimates

WOCS ID	WD Temp (K)	Age (Myr) <sup>a</sup>	Period (days) <sup>b</sup>	Eccentricity <sup>b</sup>
4348	13000 ± 500	230 ± 30	1168 ± 8	0.09 ± 0.05
4540	18100 ± 500	70 ± 7	3030 ± 70	0.36 ± 0.07
5350	13200 ± 500	220 ± 30	690 ± 3	0.07 ± 0.05
5379	17600 ± 500	77 ± 7	120.21 ± 0.04	0.24 ± 0.03

Notes.

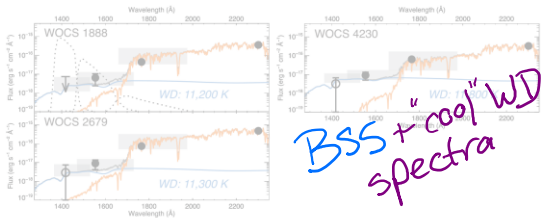
<sup>a</sup> Holberg & Bergeron (2006); Tremblay et al. (2011).<sup>b</sup> Geller et al. (2009).

Figure 3. Best-fit BSS + WD spectra for the three BSSs with cool (11,000–12,000 K) WD companions, as labeled. The colors and symbols used are the same as in Figure 2. For sources without a F140N detection the 3 $\sigma$  upper limit is shown with a black bar and a down arrow. Due to the fainter WD flux these three BSSs have WD companions detected at the  $>2$  level. The WD temperatures here correspond to ages between 310 and 360 Myr (Holberg & Bergeron 2006; Tremblay et al. 2011).

## The other sources

lack a WD companion. The possibility remains that some of these BSSs have a cool WD companion because 11,000–12,000 K WD temperatures are often observed. This emission is generally bluer and brighter than the expected emission for that particular BSS. For example, WOCS 2679 has a temperature of approximately 11,000 K. Such a WD is likely to have enough FUV emission to drown the WD flux for any BSS in NGC 188.

We investigated whether any of the 12 FUV-faint BSSs are accompanied by modeling the expected photometry for each BSS individually. Following a similar methodology as in Section 3.2, for each individual FUV-faint BSS we do a Monte Carlo sampling of the temperature ranges and WD luminosities. We then compare the resulting two-dimensional density distribution with the F150N – F160M – F165L for that particular BSS. We then find the model density value with the same color and magnitude as the BSS observation. We then take that value as the probability that the BSS has a cool WD companion ( $P_{\text{BSS}}$ ). The probability that the BSS has a WD companion is then  $P_{\text{BSS}} \times P_{\text{WD}}$ .

The modeled photometric for each BSS is highly dependent on the temperature range and WD luminosity. The NUV

luminosity used to normalize the model spectra. We compared the temperature used here with recorded WD temperatures obtained from the nine-epoch HST data. In Table 5, private communication, many BSS temperatures are consistent across the methods, i.e., WOCS 1888 and 4581 have temperatures consistent with the WD temperatures of approximately 11,000 K. Additionally, temperatures for WOCS 2679 vary. BSS WD temperatures vary by 200–300 K. If the actual WD temperature is different from the modeled BSS temperature, the observed BSS photometry could mimic the presence of a cool WD companion. In order to account for potential offsets in the known temperatures, and avoid false identification of a WD companion, we also model each BSS with temperature ranges shifted by  $\pm 200$  K and adopt the highest  $P_{\text{BSS}}$ , allowing for each BSS.

In Table 4 we list the 12 FUV-faint BSS along with the probability that they have a cool WD companion between 11,000 and 12,000 K. There are three BSS with probabilities greater than 90%: WOCS 1888 ( $P_{\text{WD}} = 96\%$ ), WOCS 2679 ( $P_{\text{WD}} = 95\%$ ), and WOCS 4230 ( $P_{\text{WD}} = 95\%$ ). The photometry for WOCS 1888, 2679, and 4230 are best fit with WD composite spectra with WD temperatures between 11,000 and 12,000 K, as shown in Figure 3. The best-fit periods and corresponding ages for these sources along with binary orbital parameters are given in Table 4. There is a 2% chance the total of the 12 FUV-faint BSSs have WDs equal to or older than 96% due to random chance.

WOCS ID	Binary probabilities											
	451	1888	2679	4230	4290	4306	4581	4970	5020	5325	5671	8104
$P_{\text{WD}}$	0.13	0.96	0.97	0.99	0.63	0.74	0.56	0.79	0.92	0.81	0.70	0.10

## "cool" WD parameters

WOCS ID	WD Temp (K)	Age (Myr) <sup>a</sup>	Period (days) <sup>b</sup>	Eccentricity <sup>b</sup>
1888	11200 ± 500	360 ± 50	2240 ± 30	0.21 ± 0.04
2679	11300 ± 500	350 ± 50	1033 ± 8	0.07 ± 0.05
4230 <sup>c</sup>	11800 ± 500	310 ± 40	...	...

Notes.

<sup>a</sup> Holberg & Bergeron (2006), Tremblay et al. (2011).

<sup>b</sup> Geller et al. (2011).

<sup>c</sup> Holberg & Bergeron (2006) has a third binary companion due to a mass transfer event (Geller et al. 2009).

2% chance of  $\frac{1}{3}$  being wrong, 0.03% chance of  $\frac{3}{3}$  being wrong!

BSS ages estimated  $\sim 360$  Myrs

How often does MT occur?

In Figure 5 optical CMD of NGC 188 is shown. The HST photometry reveals four hot WD companions that are hotter than 12,000 K, as three visual WD companions and one non-velocity variable BSS. All of the detected WDs are in own 1–2 Myr. This result may include the presence of cold WD companions (temperatures less than 11,900 K) among the remaining BSSs, but we are unable to identify cold WD companions using these photometric data.

In Figure 6 we plot an optical CMD ( $V - B - V$ ) of NGC 188. Use location on CMD to probe relation of age vs. luminosity/color. Ages along ZAMS is 77–360 Myrs. We compare with a theoretical CMD calculation of BSSs with detected WD companions to probe relationships between BSS age and optical luminosity and color. Several young (down to the ZAMS) and old (up to 360) of the BSSs with hot WD companions (WOCS 4230 and 5379), two of the BSSs with cool WD companions (WOCS 2679 and

4230) and an additional binary with a 10% probability of having a third companion. Based on the theoretical WD isochrones, the mass of a star along the ZAMS is 77–360 Myr (Holberg & Bergeron 2006; Tremblay et al. 2011), and may extend further. WOCS 8104 has cool WD components.

At the same time, two of the youngest mass-transfer-formed BSSs (WOCS 4540 and 5350) lie well off the ZAMS.

The results show that BSS populations may impact the evolution of the ZAMS in the population, but distance from the ZAMS is not necessarily equivalent with age since formation. One must take into account the age of BSSs using single-star isochrones, especially for BSSs that lie away from the ZAMS.

Test the frequency velocity variable BSSs in the optical CMD of the cluster. There are 10 BSSs formed through collisions that would likely be among the most massive BSSs. These are located in the high-luminosity region (Leigia et al. 2011). And yet, there are more luminous than the most luminous mass-transfer-formed BSS. These are located in the high-luminosity region. These may be transfer BSSs and possible collision BSSs in the optical CMD.

Frequency BSS formation through MT

Previous work (mainly by Mathieu & Geller 2009; Geller & Mathieu 2011) has shown WDs detected in mass transfer to be more common than WDs formed through mass transfer. Older, mass-transfer-formed BSSs have cold WD companions that are consistent with the mass of a star along the ZAMS. Younger mass-transfer-formed BSSs are greater than seven. Therefore, our results confirm previous predictions that the majority of young BSSs in 188 form through mass transfer.

We can further constrain the total frequency of mass-transfer formation by considering how many BSSs may form through other mechanisms.

We do not expect any of the velocity variable BSSs to form through Case B or C Roche lobe overflow mass transfer. As noted, velocity variable BSSs are either single stars or binaries with orbital periods greater than

Mass transfer (more than half)

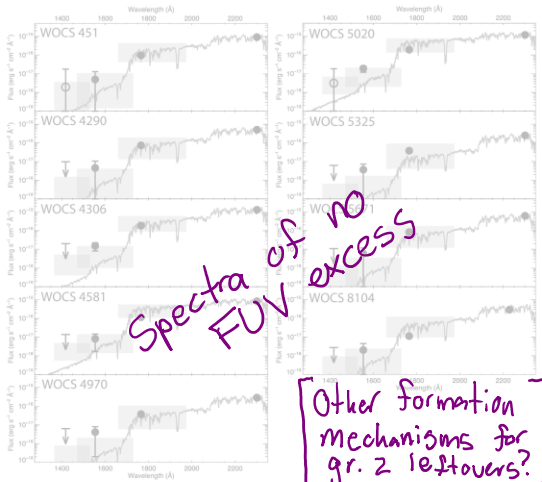


Figure 4. Best-fit spectra for the BSSs without significant FUV excesses. The colors and symbols used are the same as in Figures 2 and 3. These sources do not have detected WD companions with temperatures of 11,000 K or greater. (The NUV point for WOCS 8104 is WFC3 F218W photometry from this study.)

10,000 days. Case C mass transfer systems have final orbital periods less than about 3000 days (Chen & Han 2008), which is well within the RV binary detection limit in NGC 188 (Geller et al. 2009). Collisional formation is a small possibility for non-variable stars in a binary system, since it is undetectable using dimpledosity methods. In addition, it is undetectable using radial velocity measurements. In this case, the discovery of a secondary in a binary system would indicate the presence of B/C velocity-variable BSSs in NGC 188 is in a binary with a period less than  $10^4$  days but is not detected due to inclination; Geller & Mathieu (2012). We present that the non-variable variable star formation is another mechanism to produce collisional BSSs from contact binaries.

Is it possible that the remaining eight SB1 BSS binaries to form through other processes? It is unlikely that the SB1 BSSs formed through collisions. BSSs formed through collisions can be in binaries, but the orbital periods tend to be very long and beyond RV sensitivity limits

**Do not expect gr. 1 to have undergone case B/C**

**No case C due to orbit limitations**

**Orbits of collision mechanisms tend to be very long and too little mass of secondaries**

**(2) Mechanism could be possible (but there is a mass difference)**

(Geller et al. 2013). In addition, given the observed statistical properties and distribution of SB1 BSS secondary masses by Geller & Mathieu (2012), with a strong peak at  $0.5 M_{\odot}$ . Models of collisionally formed BSS binaries with monolithic secondaries companion to the observed secondary in distribution allows (Geller & Mathieu 2011).

Some SB1 BSSs may be formed through Kozai-induced merger with their host cluster (Perets 2014). The resulting period distribution would be similar to that observed in the NGC 188 BSS binaries, but the secondary masses would differ (Perets 2014). The original tertiary was removed from the cluster by the Kozai effect (Perets 2014).

With no strong observational constraint, the hierarchical triple star cluster is difficult to make quantitative predictions about the nature of Kozai-formed BSSs. Nevertheless, the 2014 study of Kozai-SAS formation

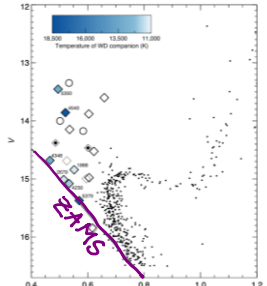


**Fig. 5 Optical CMD of NGC 188**  
Figure 5. Optical color-magnitude diagram of NGC 188. The plot shows the measured V magnitude versus the measured temperature of WD companions. The solid black line is the ZAMS for NGC 188. Binary BSSs are shown as diamonds and non-binary velocity BSSs are shown as large circles. The outlined solid black diamonds are the two double-lined BSS binaries that are not included in this *HST* study. The BSSs with WD detections are shown with a color from dark blue to light blue representing the temperature of the WD companion, as indicated with the color bar. The sources outlined in gray (two SB1 binaries, one single BSS) are the three sources without a  $3\sigma$  detection.

1500

**Group 3 BSSs are still unknown**  
with an  $N$ -body model of NGC 188 containing 200 primordial triples—essentially ~~primordial~~ planetary systems with periods between 2 and 50 years. This model creates an additional 1–2 BSSs at the age of NGC 188, but most of the BSSs are formed through triple systems, not from the Kozai mechanism itself. Approximately 0.05% of the stars in the  $N$ -body model undergo the Kozai mechanism. However, the Geller et al. (2013) Kozai model prescription is incomplete, and cannot yet predict the formation of triple systems. We estimate that one of the BSS SB1 binaries may have formed through a merger in a hierarchical system.

**To summarize:**

~~Gr. 1) No RLOF Mechanism~~

~~Gr. 2) 7/15 BSSs have a detected WD Companion establishing a 33% lower limit to ③ mechanism~~

**Gr. 3) Unknown**

We currently have no specific hypothesis for the formation mechanism of the two SB1 long-period BSS binaries, Case B and Case C. In addition, we have not found any short-period BSS binary with mass ratio near unity. In the case of the 15078 and 7782  $N$ -body models fail to create similar systems, even with a pulsar-like companion. These BSSs may have formed through a different mechanism than the ones we have studied. We know for certain, as they have more complex origins we exclude the same following the inferred properties and inferred population characteristics.

In summary, we detect WD companions to 7 of the 15 SB1 BSSs above 1500 K. Given the inferred properties and inferred

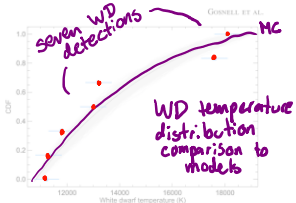


**Figure 6. CDF of detected WD temperatures compared to  $N$ -body model predictions. The distribution from the  $N$ -body model of NGC 188 is shown as a black line (Geller et al. 2013). The light gray lines are from 1000 Monte Carlo bootstrap resamples of the WD temperature distribution. The seven WDs detected in this study are shown as solid blue squares at the temperatures given in Figures 2 and 3 with 500 K error bars. A KS test indicates the CDF of the detected WD temperatures is consistent with being drawn from the same parent population in the  $N$ -body model distribution ( $p = 0.97$ ).**

but due to the binary props...

companion masses of the remaining SB1 BSSs in NGC 188, our investigation of the currently hypothesized formation mechanisms suggests that 14 SB1 BSSs were formed through mass transfer. Thus, 14 of the 21 BSSs likely formed through mass transfer, for a total BSS mass-transfer formation frequency in NGC 188 of approximately 67%.

## 4.2. Population models

Now that other BSS formation scenarios have been considered we can make an appropriate comparison between our empirical results and the theoretical results of the Geller et al. (2013)  $N$ -body model of NGC 188. Geller et al. (2013) present 20 full-lifetime  $N$ -body realizations of NGC 188, with constraints of the same as the  $N$ -body model dynamical encouters. The model was able to track the evolution of all BSSs and retain information on where the mass transfer ended in each system.

With 14 WD detections we can directly compare the empirical and theoretical age distributions for mass transfer-forming BSSs. We take the black body temperature distribution for all mass transfer ended WDs and convert the time since mass transfer ended to a WD temperature (Holberg & Bergeron 2006; Tremaine et al. 2013). We then repeat the process in Figure 6 as a solid black line with light gray lines representing Monte Carlo bootstrap resampling of the  $N$ -body CDF, meant to illustrate the inherent scatter in the empirical distribution.

We compare the  $N$ -body age distribution to the empirical age distribution, shown in Figure 6 as blue squares with 500 K error bars. A KS test shows the empirical distribution and theoretical distribution are consistent with being drawn from the same parent distribution ( $p = 0.97$ ). The overall shape of the  $N$ -body age distribution is fully consistent with the BSS ages detected in this study.

Adopting a mass-transfer formation frequency of 67% for the BSS population implies there are five BSSs in NGC 188 that formed through other formation mechanisms, such as collisions or the Kozai mechanism, in addition to the two short-

period SB2 systems. This *number* is consistent with the number of collisionally formed BSSs seen in the Geller et al. (2013) *N*-body model of NGC 188.

The *fraction* of collisionally formed BSSs in the Geller et al. (2013) study is quite different than observed, however, because the total number of BSSs created is too low. The model results have an average of six BSSs in NGC 188 at 7 Gyr, one of which formed from mass transfer. A separate *N*-body study of the open cluster M67 also fails to create a high fraction of mass transfer-formed BSSs as observed in NGC 188 (Hurley et al. 2005), although the progenitor binary period distributions used were not realistic.

The lack of BSSs in *N*-body models (Geller et al. 2013) may be attributed to an incomplete description of mass transfer processes in the binary population synthesis models used within the *N*-body code. Geller et al. (2013) utilize the NBODY6 code (Aarseth 2003), which relies similar algorithms to those implemented in the Binary Stellar Evolution (BSE) code of Hurley et al. (2002) to track binary evolution.

Although there are too few BSSs, Geller et al. (2013) note that the model produces a large number of long-period post-common envelope (CE) binaries that are not observed at such frequency in NGC 188 or the field. The mass transfer parameterization in BSE may need to be adjusted such that these sources go through stable Roche lobe overflow rather than CE. Converting the post-CE binaries to BSS+WD binaries would bring the total mass transfer BSS population to 10 systems at 7 Gyr, for a mass-transfer formation frequency of 67%. This matches the inferred mass-transfer formation frequency of 67% measured in this study for the total NGC 188 BSS population.

However, if the parameterization of mass transfer is amended in BSE the consistency of the age distributions from the *N*-body model and these results should be revisited.

Binary population synthesis models are important tools for theoretical astronomy that allow full-*N* models of rich open clusters to run in a reasonable amount of time. We hope that observations such as these help constrain the parameterizations used so that population synthesis models can be as accurate as possible.

## Summary

We utilize a FUV photometric study of the BSS binaries in the open cluster NGC 188 to search for FUV excesses from WD companions in binary systems formed through mass transfer. We detect four BSSs with host temperatures greater than 12,000 K, WD companions. Since WDs are the remnants of stars that have already exhausted the fuel in their cores, we can place limits on the WD ages. These four systems are younger than 250 Myr, indicating the mass transfer event occurred in the recent past. By comparing the expected and observed FUV emission on a star-by-star basis with the H $\alpha$  BSS temperatures, we find that three of the systems detected have additional FUV counterparts that imply host temperatures between 11,000 and 18,000 K. These three systems are likely to be BSSs formed through mass transfer in the past 400 Myr. Analyzing the location of these newly formed BSSs in the optical CMD reveals that the youngest BSSs are located near the ZAMS, while BSSs near the ZAMS are likely among the youngest of the population, distance from the ZAMS is not a direct indicator of BSS age. Single-star isochrones may not be

(33%)

**Seven BSS + WD were found with HST data, which suggests very recent mass transfer**

After determining the orbital periods of the BSSs, we do not yet understand the evolution of the optical CMD between mass transfer-formed BSSs and the single variable BSSs possibly formed through collisional mergers of contact binaries.

The current *Hubble* study sets the upper limit of 33% for the mass transfer formation frequency of BSSs in NGC 188. In addition, we explore the possibility of other formation mechanisms for BSSs and their propagation in BSS population to theoretical predictions. Due to the BSS formation mechanism, it is very unlikely that most of the BSSs formed through dynamical collisions. Collisions typically create either single BSSs or BSSs with long periods that are spectroscopically with RVs (Geller et al. 2013). It is unlikely that all of the BSSs are variable BSSs formed through collisions, as the BSSs in the field are mostly short-period, most often binaries with periods well within our RV detection limits (Chen, Hurley, & Geller 2014). Using an *N*-body simulation (Geller et al. 2013), we predict that the likely mechanism for forming 0.5 BSSs at the age of NGC 188 is that we assume that one SB1 binary merged to form a triple via the Kozai-Lidov mechanism. As a result, we find that 14 of the 15 SB1 BSSs likely formed through mass transfer. This results in a total mass-transfer formation frequency of approximately 67% (13/19) for BSSs in NGC 188. These results strongly support the previous predictions in Mathieu & Geller (2013) and Geller & Mathieu (2014) at the core of the NGC 188 cluster form through mass transfer.

The distribution of BSS ages found in this study is consistent with the formation mechanism. The distribution of mass-transfer formed BSSs in the *N*-body simulations of Chen et al. (2014) shows a frequency of mass transfer formed BSSs. We find here that the results of *N*-body models that have difficulty creating numerous mass transfer BSSs (Hurley et al. 2005) are problematic. It is possible that the poor resolution of unstable mass transfer causes too many BSS-progenitor binaries to go into a state of CE rather than the long-period CE overflow. If the parameterization within the *N*-body model of NGC 188 was adjusted such that the long-period CE systems instead went through stable mass transfer, the model would reproduce the BSS mass-transfer formation frequency measured in this study.

Ruling out other formation mechanisms, 9/14/21 BSSs are born through MT. 67% The why

**These BSS+WD binary detections represent some of the most well-characterized post-mass transfer systems to date, and provide an unparalleled opportunity to constrain detailed mass transfer and binary evolution models (Gosnell et al. 2014).** These BSS+WD binaries will also help address the discrepancy between observations and *N*-body and population synthesis results.

We are grateful to the anonymous referee whose comments and suggestions improved this work. We thank K. Milliman for sharing the H $\alpha$  BSS temperatures before publication. We are extremely grateful to P. Bergeron for sharing his grid of WD atmosphere models. N.M.G. acknowledges support from the W. J. McDonald Postdoctoral Fellowship. R.D.M. and N.M.G. (while previously at UW-Madison) are supported through *HST* Program number 12492, provided by NASA through a grant from the Space Telescope Science Institute, which is operated by the Association of Universities for Research in Astronomy, Incorporated, under NASA contract NAS5-26555. A.S. is supported by the Natural Sciences and Engineering Research

Council of Canada. A.M.G. is funded by a National Science Foundation Astronomy and Astrophysics Postdoctoral Fellowship under award No. AST-1302765.

## REFERENCES

- Aarseth, S. J. 2003, Gravitational N-Body Simulations (Cambridge: Cambridge Univ. Press)
- Antonini, F., Chatterjee, S., Rodriguez, C. L., et al. 2015, arXiv:1509.05080
- Boffo, F. R., Sirianiti, M., Lucas, R. A., Walborn, N. R., & Profitt, C. R. 2008, *Tech. Instrument Rep. ACS* 2008-002 (<http://www.stsci.edu/hst/acs/documents/tirs/irf802.pdf>)
- Burbidge, E. M., & Sandage, A. 1958, *ApJ*, 128, 174
- Carney, W. H., Latham, D. W., Laird, J. B., Grant, C. E., & Morse, J. A. 2001, *AJ*, 122, 3419
- Castelli, F., & Kumez, R. L. 2004, arXiv:astro-ph/0409087
- Chen, X., & Han, Z. 2008, *MNRAS*, 387, 1416
- Dieball, A., Knigge, C., Zurek, D. R., et al. 2005, *ApJ*, 634, L105
- Feldman, P. D., Weaver, H. A., Saar, J., & McGrath, M. A. 2010, Hubble after SM4: Preparing JWST, 31
- Ferraro, F. R., Beccari, G., Daleyandrea, E., et al. 2009, *Nature*, 462, 1028
- Ferraro, F. R., D'Amico, N., Pousset, A., et al. 2001, *ApJ*, 561, 337
- Ferraro, F. R., Fusi Pecci, F., Bellazzini, M., et al. 1995, *A&A*, 294, 80
- Ferraro, F. R., Palmaieri, B., Roed, R. T., & Dorman, B. 1999, *ApJ*, 522, 983
- Ferraro, F. R., Sabbi, E., Gratton, R., et al. 2006, *ApJ*, 647, 53
- Geller, A. M., Hurley, J. R., & Mathieu, R. D. 2013, *AJ*, 145, 8
- Geller, A. M., & Mathieu, R. D. 2011, *Nature*, 478, 356
- Geller, A. M., & Mathieu, R. D. 2012, *AJ*, 144, 54
- Geller, A. M., Mathieu, R. D., Harris, H. C., & McClure, R. D. 2008, *AJ*, 135, 2264
- Geller, A. M., Mathieu, R. D., Harris, H. C., & McClure, R. D. 2009, *AJ*, 137, 3743
- Gonzaga, S. 2014, ACS Data Handbook, Version 7.1 (Baltimore: STScI)
- Gosnell, N. M., Mathieu, R. D., Geller, A. M., et al. 2014, *ApJL*, 783, L8
- Henden, A., & Munari, U. 2014, CoSka, 43, 518
- Hollberg, J. B., & Bergeron, P. 2006, *AJ*, 132, 1221
- Hurley, J. R., Pols, O. R., Aarseth, S. J., & Tout, C. A. 2005, *MNRAS*, 363, 293
- Hurley, J. R., Tout, C. A., & Pols, O. R. 2002, *MNRAS*, 329, 897
- Johnson, H. L., & Sandage, A. R. 1955, *ApJ*, 121, 616
- Knigge, C., Dieball, A., Maza Apellániz, J., et al. 2008, *ApJ*, 683, 1006
- Knigge, C., Gilliland, R. L., Dieball, A., et al. 2006, *ApJ*, 641, 281
- Knigge, C., Leigh, N., & Sills, A. 2009, *Nature*, 457, 288
- Kroupa, P. 2001, *MNRAS*, 322, 231
- Leigh, N., & Geller, A. M. 2012, *MNRAS*, 425, 2369
- Leigh, N., Knigge, C., Sills, A., et al. 2013, *MNRAS*, 428, 897
- Leigh, N., & Sills, A. 2011, *MNRAS*, 410, 2370
- Leigh, N., Sills, A., & Knigge, C. 2007, *ApJ*, 661, 210
- Leigh, N., Sills, A., & Knigge, C. 2011, *MNRAS*, 416, 1410
- Leonard, P. J. T. 1989, *ApJ*, 98, 217
- Leonard, P. J. T. 1996, *ApJ*, 470, 521
- Lombardi, J. C., Jr., Warren, J. S., Rasio, F. A., Sills, A., & Warren, A. R. 2002, *ApJ*, 568, 939
- Mapelli, M., Ripamonti, E., Tolstoy, E., et al. 2007, *MNRAS*, 380, 1127
- Mapelli, M., Sigurdsson, S., Ferraro, F. R., et al. 2006, *MNRAS*, 373, 361
- Martin, D. C., Fanson, J., Schiminovich, D., et al. 2005, *ApJL*, 619, L1
- Mathieu, R. D. 2000, in ASP Conf. Ser. 198, Stellar Clusters and Associations: Convection, Rotation, and Dynamos, ed. R. Pallavicini, G. Micela & S. Scuderi (San Francisco, CA: ASP), 517
- Mathieu, R. D., & Geller, A. M. 2009, *Nature*, 462, 1032
- Mathieu, R. D., & Geller, A. M. 2014, in Ecology of Blue Stragglers, ed. H. Boffin, G. Carraro & G. Beccari (Berlin: Springer-Verlag), 29
- McCracken, W. H. 1964, *MNRAS*, 128, 147
- Meibom, S., Grundahl, F., Clausen, J. V., et al. 2009, *AJ*, 137, 5086
- Morony, Y., Held, E. V., Saviane, I., et al. 2007, *A&A*, 468, 973
- Naoz, S., & Fabrycky, D. C. 2014, *ApJ*, 793, 137
- Perts, H. B. 2014, in Ecology of Blue Stragglers, ed. H. Boffin, G. Carraro & G. Beccari (Berlin: Springer-Verlag), 251
- Perts, H. B., & Fabrycky, D. C. 2009, *ApJ*, 697, 1048
- Piotto, G., De Angeli, F., King, I. R., et al. 2004, *ApJL*, 604, L109
- Platais, I., Koizumura-Platais, V., Mathieu, R. D., Girard, T. M., & van Altena, W. F. 2003, *AJ*, 126, 2922
- Preston, G. W., & Sneden, C. 2000, *AJ*, 120, 1014
- Ramírez, I., & Meléndez, J. 2005, *ApJ*, 626, 465
- Rodríguez-Merino, L. H., Chavez, M., Bertone, E., & Buzzoni, A. 2005, *ApJ*, 626, 411
- Rozyczka, M., Kaluzny, J., Thompson, I. B., et al. 2013, *AcA*, 63, 67
- Rucinski, S. M. 2000, *AJ*, 120, 319
- Sandage, A. R. 1953, *AJ*, 58, 61
- Sandquist, E. L. 2005, *ApJL*, 635, L73
- Santana, P. A., Munoz, R. R., Geha, M., et al. 2013, *ApJ*, 774, 106
- Saragelidze, A., von Hippel, T., Koizumura-Platais, V., & Demargue, P. 1999, *AJ*, 118, 2894
- Skrutskie, M. F., Cutri, R. M., Stiening, R., et al. 2006, *AJ*, 131, 1163
- Talamantes, A., Sandquist, E. L., Clem, J. L., et al. 2010, *AJ*, 140, 1268
- Tian, B., Deng, L., Han, Z., & Zhang, X. B. 2006, *A&A*, 455, 247
- Tremblay, P.-E., Bergeron, P., & Gianninas, A. 2011, *ApJ*, 730, 128
- Webbink, R. F. 1976, *ApJ*, 209, 829
- Wood, M. A. 1995, in 9th European Workshop on White Dwarfs, ed. D. Koester & K. Werner (Berlin: Springer-Verlag), 41